

## Electronic Supplementary Information

### **Membrane destabilization by monomeric hIAPP observed by Imaging Fluorescence Correlation Spectroscopy**

**Nirmalya Bag,<sup>a</sup> Ashraf Ali,<sup>b</sup> Virander Singh Chauhan,<sup>b</sup> Thorsten Wohland<sup>\*a</sup> and Aseem Mishra<sup>\*b</sup>**

<sup>a</sup>Departments of Biological Sciences and Chemistry and NUS Centre for Bio-Imaging Sciences (CBIS), National University of Singapore, Singapore 117557

<sup>b</sup>Malaria Research Group, International Centre for Genetic Engineering and Biotechnology, Aruna Asaf Ali Marg, New Delhi, India 110067

Corresponding authors' e-mails:

[twohland@nus.edu.sg](mailto:twohland@nus.edu.sg)

[assem@icgeb.res.in](mailto:assem@icgeb.res.in)

## Table of Contents

Glossary of terminology .....	3
Chemical and Reagents.....	3
Synthesis of human Islet Amyloid Polypeptide (hIAPP) .....	3
hIAPP Peptide stock solution.....	3
Aggregation of hIAPP.....	4
Transmission Electron Microscopy (TEM) .....	4
Preparation of rhodamine labeled vesicles (RLVs) .....	4
Preparation of rhodamine entrapping vesicles (REVs).....	4
Preparation of supported lipid bilayers (SLBs) .....	4
Cell culture.....	4
UV-Vis spectroscopy .....	5
Fluorescence spectroscopy.....	5
Circular Dichroism (CD) .....	5
Confocal fluorescence correlation spectroscopy (FCS) set up, data acquisition and data analysis	5
Determination of the mode of interaction of peptide with membrane by diffusion time measurements of REV and RLV.....	6
Imaging total internal reflection-fluorescence correlation spectroscopy (ITIR-FCS) set up, data acquisition and data analysis.....	6
Principle of FCS Diffusion Law implemented in ITIR-FCS .....	7
Figure S1 .....	9
Figure S2.....	10
Figure S3.....	11
Figure S4.....	12
Figure S5.....	13
Figure S6.....	14
Figure S7.....	15
Figure S8.....	16
Figure S9.....	17
Figure S10.....	18
Supporting information videos .....	19
Acknowledgements.....	19

### **Glossary of terminology**

DOPC: 1,2-dioleoyl-*sn*-glycero-3-phosphocholine

DPPC: 1,2-dipalmitoyl-*sn*-glycero-3-phosphocholine

Chol: Cholesterol

RhoPE: 1,2-dimyristoyl-*sn*-glycero-3-phosphoethanolamine-N-(lissamine rhodamine B sulfonyl) (ammonium salt)

### **Chemical and Reagents**

All chemicals and reagents were purchased from Sigma-Aldrich (Singapore) (unless otherwise mentioned). Lipids were procured from Avanti Polar Lipids (Alabaster, AL).

### **Synthesis of human Islet Amyloid Polypeptide (hIAPP)**

The peptide was synthesized on Rink Amide-MBHA resin (Novabiochem, USA) (100-200 mesh, substitution level ~0.4 mM/g) at a scale of 0.1 mM. The method of solid phase peptide synthesis was used with N-terminal base labile Fmoc- and acid labile side-chain protections (Novabiochem, USA). As a standard procedure, double re-coupling was done while the state of N-terminal protection/deprotection was assessed carefully with Kaiser test. 4-5 rounds of recoupling was done after resin was washed with DCM:DMF (1:1) wherever coupling was difficult. Heating the reaction to 40 °C enhanced the coupling efficiency considerably. The sequence was confirmed at various points by mass spectrometry analysis during synthesis. The peptide was cleaved from the resin (95% TFA, 2.5% Thioanisole, 2.5% water), precipitated (3×) with cold diethyl ether. It was then purified on analytical scale and ES<sup>+</sup>/MS spectrum was used as an indicator of its identity and purity. ES<sup>+</sup>/MS result has been provided in Sup SI 8. Fluorescent-labeled analog was generated by coupling Rho6G-NHS ester (Atto-Tec GmbH) to the N-terminus of the growing peptide chain, before its cleavage from the resin.

### **hIAPP Peptide stock solution**

hIAPP (dry powder) was weighed accurately into a glass vial or polypropylene microfuge tube. Desired amount of 1,1,1,3,3,3-Hexafluoro-2-propanol (HFIP) was added. The peptide does not readily dissolve. Therefore, the solution was heated at 45 °C for 30 min (Caution: Boiling Point of HFIP is 55 °C. Vapors cause build up of pressure inside the tube that can explode.) Immediately after cooling, the solution was filtered by a 0.45 μ Teflon filter very slowly. Other filter materials (nylon, cellulose) are not compatible with HFIP. The clear solution can be stored at RT/4 °C for more a week without loss of reproducibility. The upper limit of stock concentration is 4 mM. (Note: hIAPP can very well be dissolved in DMSO. However, it is difficult to remove DMSO by evaporation).

### **Aggregation of hIAPP**

hIAPP readily aggregates in aqueous medium. We initiate aggregation by adding the desired amount of stock solution to buffer (10 mM HEPES, 150 mM NaCl, pH 7.4; use NaHCO<sub>3</sub> for neutralization). The preparation is aged at 37 °C for the duration required.

### **Transmission Electron Microscopy (TEM)**

The samples were spotted by placing a 20 µL drop of the aggregate preparation on a carbon-coated 300 mesh copper grid with formvar support. Excess fluid was drained off after 5 min. Negative staining was achieved with 0.2% Uranyl Acetate (aq) for 10 s. The grid was washed once to remove excess stain and imaged immediately on a 120KV Tecnai G2 (FEI, Netherlands).

### **Preparation of rhodamine labeled vesicles (RLVs)**

Calculated amounts of the lipids and dye (the final concentration of total lipid and dye was 500 µM and 30 nM respectively.) were taken in a cleaned round bottom flask. They were mixed well and then evaporated in a rotary evaporator (Rotavap R-210, Buchi, Switzerland) for 3 hours to create a thin lipid film. This lipid film is resuspended in buffer (10 mM HEPES and 150 mM NaCl, pH 7.4) to obtain a milky solution of multilamellar vesicles. This suspension was sonicated using a bath sonicator (FB15051 Model, Fisher Scientific, Singapore) until clarity to form large unilamellar vesicles. These are used as RLV in confocal FCS measurements.

### **Preparation of rhodamine entrapping vesicles (REVs)**

The protocol of the preparation of REV is similar to that of RLV. The lipids (without the dye) were resuspended in the same buffer as above containing 1 µM rhodamine 6G after evaporation of chloroform. This solution is sonicated similarly to get rhodamine entrapping large unilamellar vesicles. Then the whole solution is gel filtrated using MicroSpin™ S-200 HR Columns (GE healthcare, Singapore) to remove the non-entrapped rhodamine 6G molecules. This solution was used as REV in the confocal FCS experiments.

### **Preparation of supported lipid bilayers (SLBs)**

200 mL of the RLV obtained by the above described procedure was deposited on freshly cleaned glass coverslide (24×50-1, Fisher Brand Microscope cover glass, Fisher Scientific, Singapore). This was incubated at 65 °C for 20 min followed by cooling at room temperature for 20 min. Then the unfused vesicles were removed by washing with the same buffer about 50 times. This was then allowed to equilibrate at 37 °C for 45 min before the experiment.

### **Cell culture**

SH-SY5Y, CHO, RIN-5Fm cells were cultured in DMEM. For FCS measurements, there were plated in 8 well Nunc chambers and grown to a 60% confluency. The cells were stained with 50 nM DiI-C<sub>18</sub> solution prepared in phenol free DMEM for 45-60 min followed by washing (2X) with phenol free culture medium.

SH-SY5Y and CHO gave similar results. RIN-5Fm did not stain strongly enough for FCS measurements. Results from SH-SY5Y treatment with hIAPP are shown in the manuscript. Similar results, as shown for SH-SY5Y and CHO, are expected for different cell lines due to the cross amyloid interactions across different cell membranes\*.

\* J. Seeliger, F. Evers, C. Jeworrek, S. Kapoor, K. Weise, E. Andreetto, M. Tolan, A. Kapurniotu, R. Winter, *Angew. Chem. Int. Ed. Engl.* **2012**, *51*, 679-683.

### **UV-Vis spectroscopy**

pFTAA was used at a concentration of 1  $\mu\text{M}$  in 1X PBS. hIAPP was added to a final concentration of 1  $\mu\text{M}$ . Peptide was incubated for 15 min before acquiring spectra. Data was acquired on a Perkin Elmer Lambda 35 UV-Vis spectrophotometer with a scan speed of 100 nm/min and slit width of 1 nm.

### **Fluorescence spectroscopy**

pFTAA was used at a concentration of 1  $\mu\text{M}$  in 1X PBS. hIAPP was added to a final concentration of 1  $\mu\text{M}$ . Peptide was incubated for 15 min before acquiring spectra. Data was acquired on a Horiba Fluorolog 3 spectrophotometer with a scan speed of 50 nm/min and excitation and emission slit width of 1 nm. Average of 2 acquisitions is presented.

### **Circular Dichroism (CD)**

All CD experiments were carried out at room temperature in a 10 mM Phosphate buffer (pH 7.0) and spectra (average of five scans) were collected using a Jasco-810 spectropolarimeter and quartz cuvette with a path length of 3 mm. CD spectra were collected between 195 to 300 nm at 0.2 nm intervals with a response time of 8 sec. CD spectra (mean residue ellipticities) are presented after subtracting the spectra of buffer alone.

### **Confocal fluorescence correlation spectroscopy (FCS) set up, data acquisition and data analysis**

Confocal FCS experiments were performed using a customized Olympus FV300 confocal laser scanning microscope (Olympus, Tokyo, Japan). The green laser beam from 543 nm helium-neon laser (Melles Griot, Singapore) was focused on the sample by a water immersion objective (60 $\times$ , NA 1.2; Olympus, Tokyo, Japan) after being reflected by a dichroic mirror (560DCLP, Omega, VT) and a scanning unit. The laser power before the objective was measured to be 25  $\mu\text{W}$ . The fluorescence signal from the sample was passed through the same objective, de-scanned and finally through a 150  $\mu\text{m}$  pinhole in the image plane to block the out-of-focus light. The light was then detected by an avalanche photodiode detector (APD) (SPCM-AQR-14; Pacer, Berkshire, UK) after passing through a band pass emission filter 595AF60 (Omega, Brattleboro, VT). The transistor-to-transistor (TTL) output signal over time from APD was processed online by a hardware corrector (Flex02-01D; Correlator.com, Bridgewater, NJ, USA) to generate autocorrelation function (ACF). The total acquisition time per measurement was 30 seconds. In general 10 measurements were taken and the average outcome was reported. All ACFs were

fitted with a 3 Dimension- 2 Particle (3D-2P) model (equation S1) by a home-written program based on Igor (Wavemetrics, Lake Oswego, OR).

$$G(\tau) = \frac{1}{N} \left[ (1 - F_2) \left(1 + \frac{\tau}{\tau_{D1}}\right)^{-1} \left(1 + \frac{\tau}{K^2 \tau_{D1}}\right)^{-1/2} + F_2 \left(1 + \frac{\tau}{\tau_{D2}}\right)^{-1} \left(1 + \frac{\tau}{K^2 \tau_{D2}}\right)^{-1/2} \right] + G_{\infty} \quad (S1)$$

$G(\tau)$  is the autocorrelation function (ACF) as a function of correlation time ( $\tau$ ).  $N$ ,  $\tau_{Di}$  and  $F_i$  are number of particle, diffusion time, and fraction of the  $i^{\text{th}}$  species respectively.  $K$  is the structure factor of the confocal volume defined as the ratio of the axial ( $z_0$ ) and radial ( $\omega_0$ ) distances where the intensity drops to  $1/e^2$  to the maximum value.

The diffusion coefficient ( $D$ ) was determined from the following equation (S2) where the  $\omega_0$  was obtained from the calibration measurement with rhodamine 6G dye in solution assuming its diffusion coefficient to be  $426 \mu\text{m}^2/\text{s}$ .

$$\tau_D = \frac{\omega_0^2}{4D} \quad (S2)$$

### **Determination of the mode of interaction of peptide with membrane by diffusion time measurements of REV and RLV**

Diffusion time of the rhodamine entrapping vesicles (REVs) and rhodamine labelled vesicles (RLVs) in presence of peptide has shown to be a very important tool to determine the mode on peptide-membrane interaction. It can distinguish between peptide induced pore formation on the membrane and detergent-like membrane rupture. If peptide induces pore formation on the vesicles, diffusion time of the fluorescent entities in the sample will be similar to that of the RLV ( $\tau_d \sim \tau_{\text{vesicles}}$ ) does not change since they probe molecules (labelled with red) still remain on the vesicles. However for REV, the entrapped probe molecules are released out in the solution if there are pores on the vesicles. Since the probe molecules diffuse much faster than the vesicles, one would observe very small diffusion time of the fluorescent particles in the sample ( $\tau_d \ll \tau_{\text{vesicles}}$ ). The scenario is different for peptide induced membrane rupture. Here for RLVs, the vesicle bound probe molecules will be released and thus the diffusion time of the sample will be much smaller than the vesicles ( $\tau_d \ll \tau_{\text{vesicles}}$ ). Similar phenomenon in terms of diffusion time of the sample will also be observed for the REVs in case of vesicle rupture. This principle is illustrated in Figure S5.

### **Imaging total internal reflection-fluorescence correlation spectroscopy (ITIR-FCS) set up, data acquisition and data analysis**

ITIR-FCS measurements were done using an objective type TIRF microscope (IX-71, Olympus, Singapore) with a high NA oil immersion objective (PlanApo, 100 $\times$ , NA 1.45, Olympus, Singapore). Excitation light from a 532 nm laser (Cobolt Samba, Sweden) was introduced to the microscope by a combination of two tilting mirrors. The light was focused on the back focal plane of the objective after being reflected by the dichroic mirror (Z488/532RPC, Semrock) and was totally internally reflected in the glass-water interface by controlling the incident angle of the excitation beam by the same combination of tilting mirrors. The immersion medium of the

objective was mineral oil (Olympus, refractive index 1.516). The fluorescence from the bilayers or the lower membrane of the cell was passed through the same objective followed by transmission through the same dichroic mirror. Finally it was imaged on the CCD chip of a cooled, back-illuminated EMCCD camera (Andor iXON 860, 128×128 pixels, Andor technology, US) after being filtered by an emission filter (Z488/532M, Semrock). Andor Solis for imaging (version 4.18.30004.0) was used for image acquisition. The kinetic mode of image acquisition was used and the ‘baseline clamp’ was always used to minimize the baseline fluctuation. The camera was operated using 10 MHz pixel readout speed. An EM gain of 200 (in a scale of 6-300) was used for all imaging. Maximum analog-to-digital gain (4.7×) and 25 μs vertical shift speed were used. The pixel side length of the CCD chip in the device is 24 μm corresponding to a pixel side length of 240 nm in the sample plane (100× magnification).

A stack of 50,000 frames were taken with 1 ms time resolution from a selected 21×21 pixels region of interest (ROI) and saved at 16-bit .Tiff file. The temporal intensity trace from each pixel was autocorrelated using multi-tau correlation scheme by ImFCS, an Igor Pro (Wavemetrics, Lake Oswego, OR) based home-written software [available at: <http://staff.science.nus.edu.sg/~chmwt/ImFCS.html>] to generate autocorrelation function (ACF). This was multiplexed for all the pixels in the ROI. Each ACF was individually fitted with the following one particle model for diffusion (equation S3) using the same software to obtain the maps of diffusion coefficient ( $D$ ) and number of particles ( $N$ ).

$$G(\tau) = \frac{1}{N} \left[ \text{erf}(p(\tau)) + \frac{1}{p(\tau)\sqrt{\pi}} (e^{-(p(\tau))^2} - 1) \right]^2 + G_{\infty}; \quad p(\tau) = \frac{a}{2\sqrt{D\tau + \sigma^2}} \quad (\text{S3})$$

$G(\tau)$  is the ACF as a function of correlation time ( $\tau$ ) and  $N$ ,  $a$ ,  $D$  and  $\sigma$  are the number of particles per pixel, pixel side length, diffusion coefficient and standard deviation of the Gaussian approximation of the microscope point spread function (PSF).  $G_{\infty}$  is the convergence value of the ACF at very long correlation time.

The main outcomes from the fitting of ACF with the theoretical model are  $D$  and  $N$ . The standard deviation (SD) of  $D$  in FCS on membrane in general is about 20%. In ITIR-FCS, the data are represented as mean  $\pm$  SD. This SD is obtained from the measurements over 441 pixels in the experiments done here. Thus it actually denotes the SD of from the distribution of 441 individual  $D$  values. Note that the standard error of the mean (SEM) for the measurements is very small ( $\sim 1\%$ ). This indicates that the data is very reproducible. However due to the heterogeneity of the system (e.g., cell membrane), the SD is as high as 20%.

Diffusion measurements on SLBs and live cells were done at 310 K. The temperature was controlled by an incubator (Live Cell Instrument, CU-109, Zeiss, Singapore). For live cells, we used an additional CO<sub>2</sub>/Air gas chamber (Live Cell Instrument, FC-5, Zeiss, Singapore) to maintain 5% CO<sub>2</sub> environment.

For time lapse diffusion imaging (Video 3), measurements were taken with 5 minutes interval using the above mentioned experimental conditions. From each of these measurements, a diffusion map was computed. This principle is demonstrated in Figure S8.

### Principle of FCS Diffusion Law implemented in ITIR-FCS

FCS diffusion law is calculated from the dependence of the transit time ( $\tau_d$ ) of tracer molecules on the observation areas on the membrane plane. For free diffusion (Brownian motion),  $\tau_d$  scales linearly with the size of the observation area ( $A_{\text{eff}}$ ) revealing a single diffusion coefficient ( $D$ )

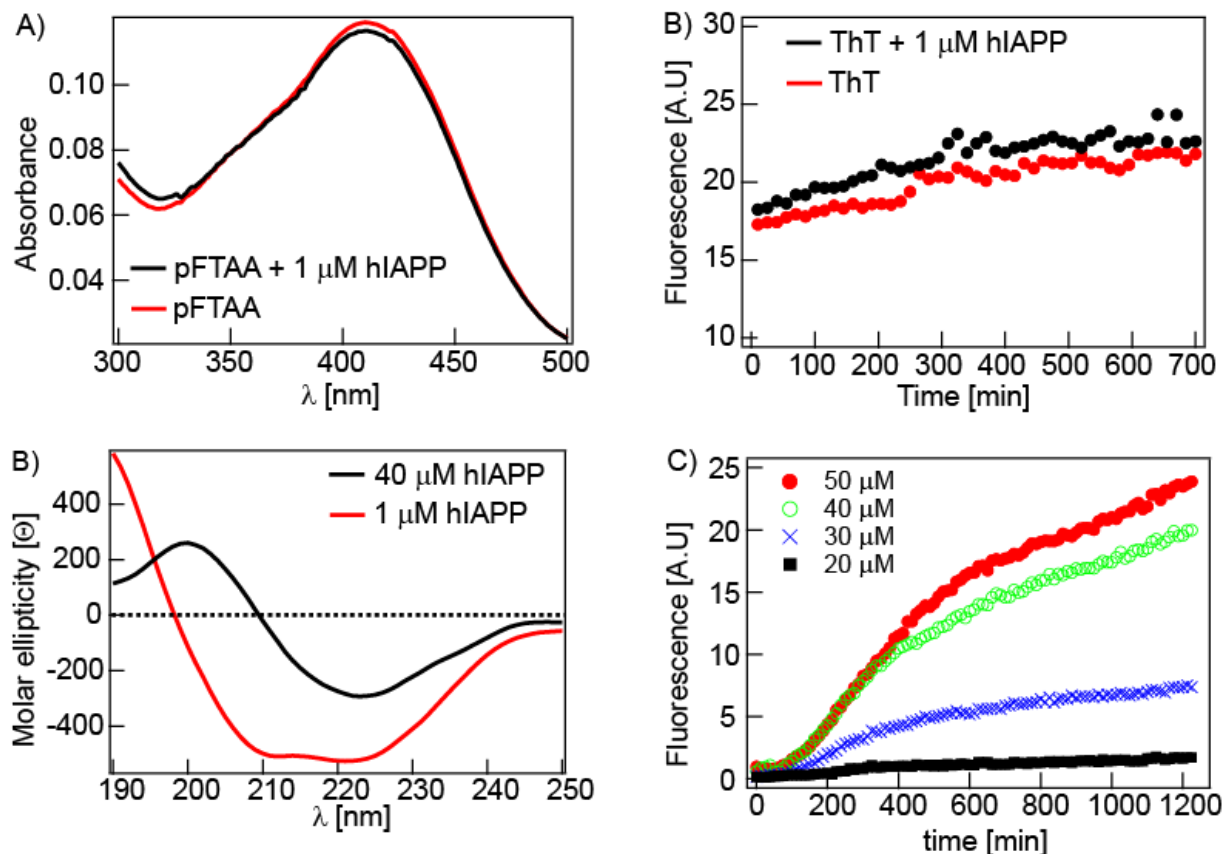
throughout. If this linear dependence of transit time on the observation area is extrapolated to zero area, the transit time will be zero as expected. However, a non-zero time at zero area reveals the heterogeneity (hindered diffusion) in the membrane under observation. Apart from free diffusion, there are two other kinds of diffusions exist in membrane, namely hop diffusion due to the cytoskeletal meshwork and hindered diffusion due to microdomains (lipid rafts). In the first case, the molecules diffuse freely within a given mesh. However, these meshes are separated by impenetrable physical barriers imposing any possible diffusion among them only through hop diffusion. The transit times obtained from probe areas containing one and many meshes respectively cannot thus be linearly scaled in the diffusion law plot as the  $D$  inside a single mesh is higher than that of the bulk membrane. In the latter scenario, partially permeable microdomains are laterally phase segregated from the rest of the membrane. The tracer molecules are either dynamically partitioned into these phases or encounter transient confinement inside the domains. This also gives a non-linear diffusion law plot since  $D$  inside domain is smaller than that of the bulk membrane. Diffraction limited observation areas created in conventional experimental set up are much larger than either of domain or mesh size, which restrains the observation of non-linearity in diffusion law plots. Thus the dependence of the  $\tau_d$  on  $A_{\text{eff}}$  which are larger than the diffraction limit can be written as the following equation:

$$\tau_d(A_{\text{eff}}) = \tau_0 + \frac{A_{\text{eff}}}{D} \quad (\text{S4})$$

For free diffusion,  $\tau_0$  is zero. However,  $\tau_0$  is strictly negative and positive values for hop diffusion in meshwork and confined diffusion in permeable microdomains respectively.

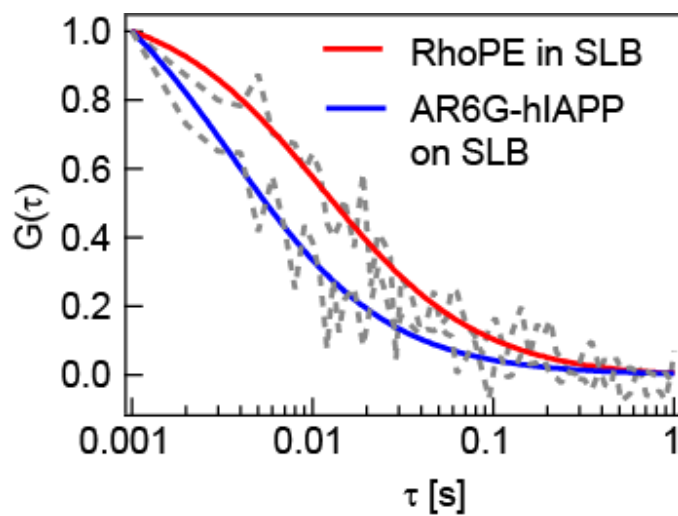
Various observation areas ( $A_{\text{eff}}$ ) are obtained from a given measurement by pixel binning (1×1 to 5×5) followed by convolution with PSF post-acquisition. Then  $D$  is determined by fitting the ACF with equation S3 for each  $A_{\text{eff}}$ . Then  $A_{\text{eff}}/D$  is plotted against  $A_{\text{eff}}$  and linearly fitted with equation S4, using the standard error of mean as weight for each point, to obtain the y-intercept  $\tau_0$ .

Figure S1



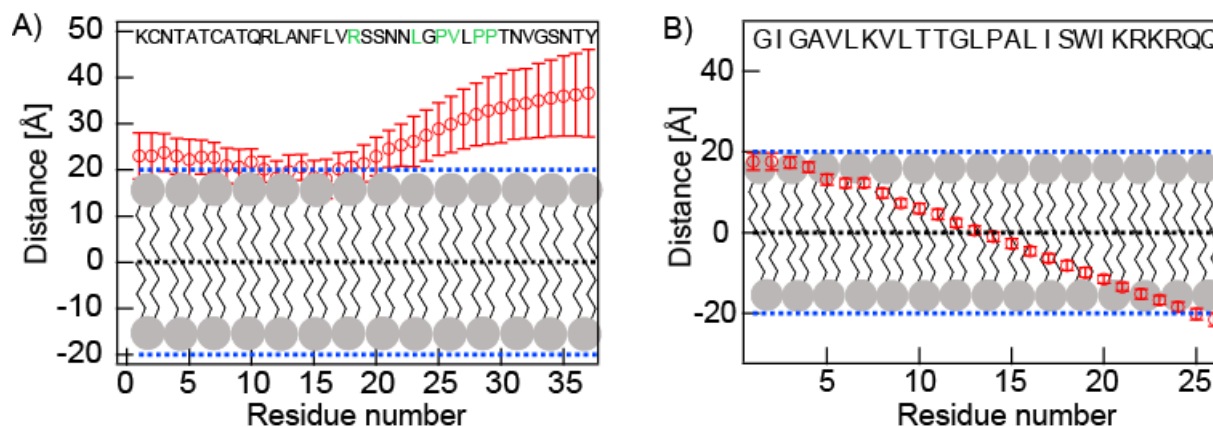
**Figure S1.** A) The UV-Vis absorption spectra of the aggregation sensing dye pFTAA in absence (blue open square) and in presence of 1  $\mu$ M (red close square) hIAPP. The identical spectra in both the conditions rule out the hIAPP aggregation. B) The fibril sensing thioflavin-T (ThT) assay does not show any aggregation (red: ThT alone and black: ThT in presence of 1  $\mu$ M hIAPP). Thioflavin T is sensitive to fibrillar structures. C) Circular dichroism (CD) spectra of 1  $\mu$ M (red) and 40  $\mu$ M (black) hIAPP. (D) The time dependent increase of ThT fluorescence of different hIAPP concentrations. There is a concentration dependent increase in relative amount of fibrils formed. At these peptide concentration (20–40  $\mu$ M) hIAPP is known to aggregate into fibres.

**Figure S2**



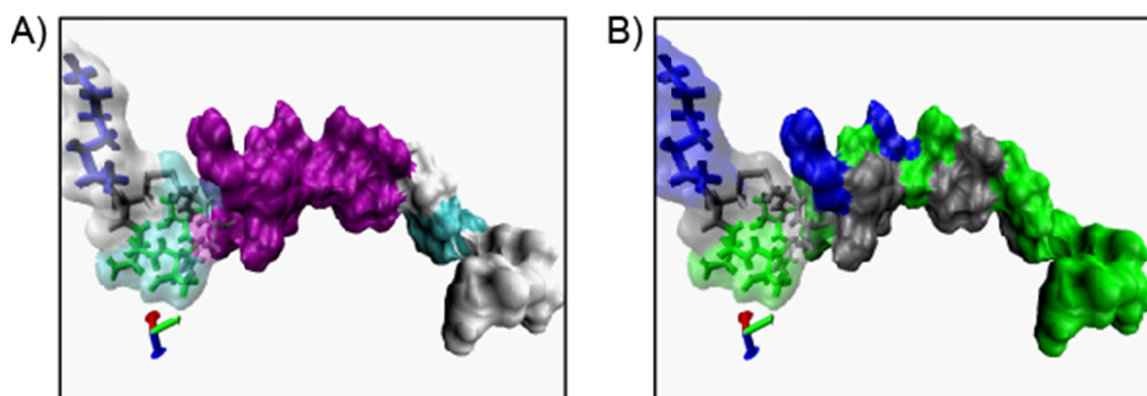
**Figure S2.** Comparison of ACFs of RhoPE in the SLB (red) and AR6G-hIAPP on the SLB (blue). AR6G-hIAPP does not insert into the membrane and thus it diffuses much faster (less wider ACF).

Figure S3



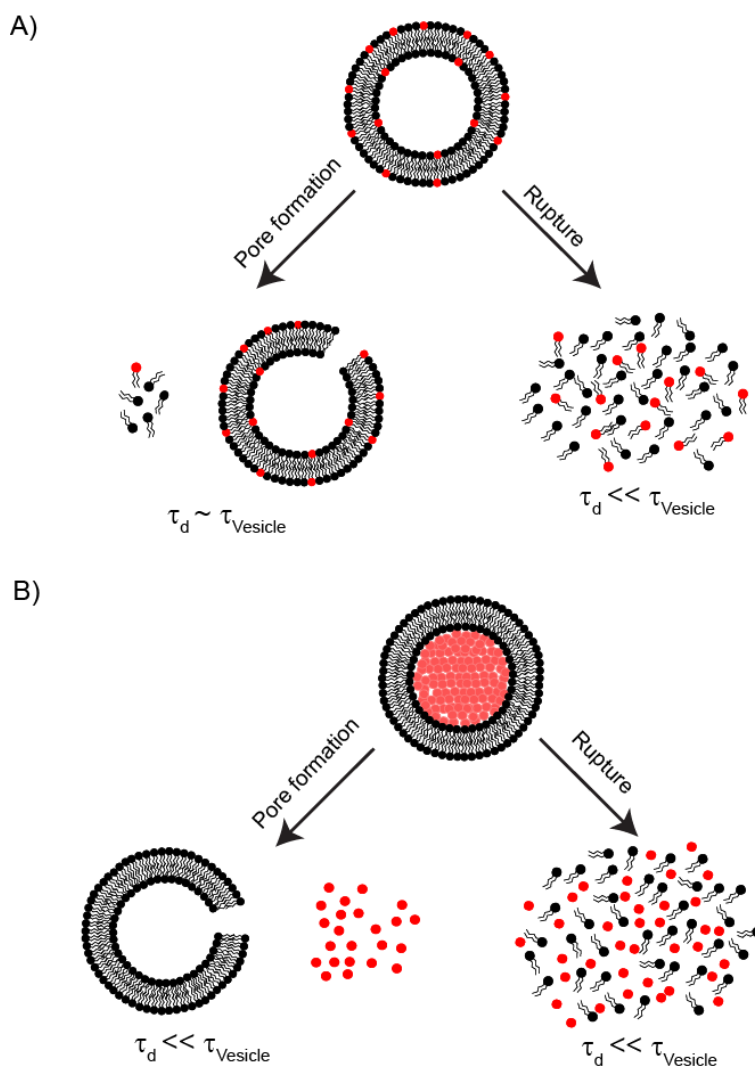
**Figure S3.** MCPep predictions of membrane association of rat IAPP (rIAPP) and mellitin are shown in figures (A) and (B) respectively. The difference in the amino acid sequence of rIAPP compared to hIAPP is shown in green in figure (A). In MCPep simulation, membrane midplane is taken a reference distance. The bilayer thickness is assumed to be 40 Å. The distance of the individual amino acids from the membrane midplane is used to predict the favorable position and association of the peptide under consideration. The simulations correctly predict weak membrane association without any insertion for rIAPP while mellitine inserts into the membrane completely.

**Figure S4**



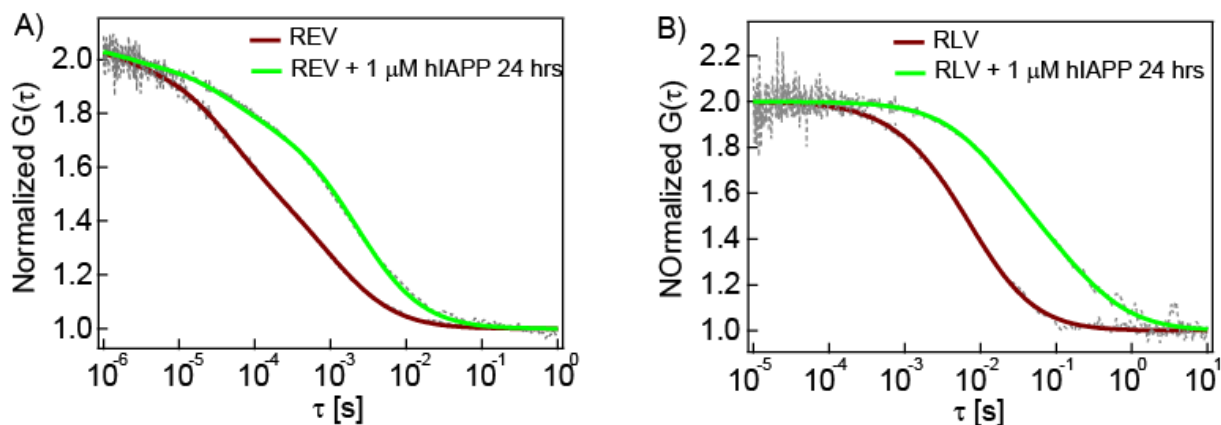
**Figure S4.** NMR derived hIAPP structure (PDB ID: 2KB8) colored according to (A) secondary structure (helical region signified in pink) (B) residue polarity (grey: hydrophobic; blue: charge, green: polar) (Transparent surface is shown for residues 1-8).

Figure S5



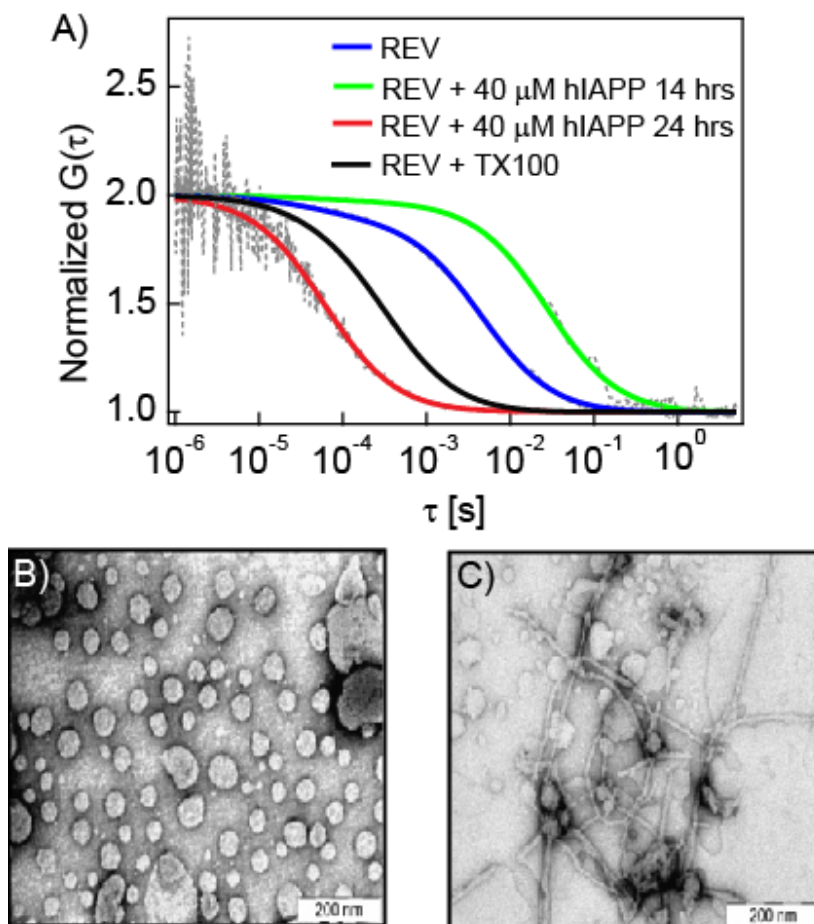
**Figure S5.** A schematic representation to discriminate the pore formation and membrane rupture mechanism from the rhodamine labeled vesicles (RLV) and rhodamine entrapping vesicles (REV) experiments. (A) Diffusion time of RLVs do not change if peptide forms pores in the membrane since there will be very little release of free dyes in the solution. Therefore, the diffusion time after peptide addition ( $\tau_D$ ) will remain same to that of vesicles ( $\tau_{\text{vesicles}}$ ). On the other hand if the peptide ruptures the membrane, all membrane bound dyes will be released in the solution. The diffusion time of the species after peptide addition ( $\tau_D$ ) will be drastically reduced compared to the vesicles ( $\tau_{\text{vesicles}}$ ). (B) The dyes entrapped inside REV will be leaked out in both the cases of pore formation and vesicle rupture. The final diffusion time ( $\tau_D$ ) will corresponds to the free dye and will be much smaller than that of vesicles ( $\tau_{\text{vesicles}}$ ). Therefore, the ‘pore formation’ and ‘detergent like rupture’ models of peptide-membrane interactions can be distinguished from these RLV and REV diffusion measurements upon addition of peptides.

Figure S6



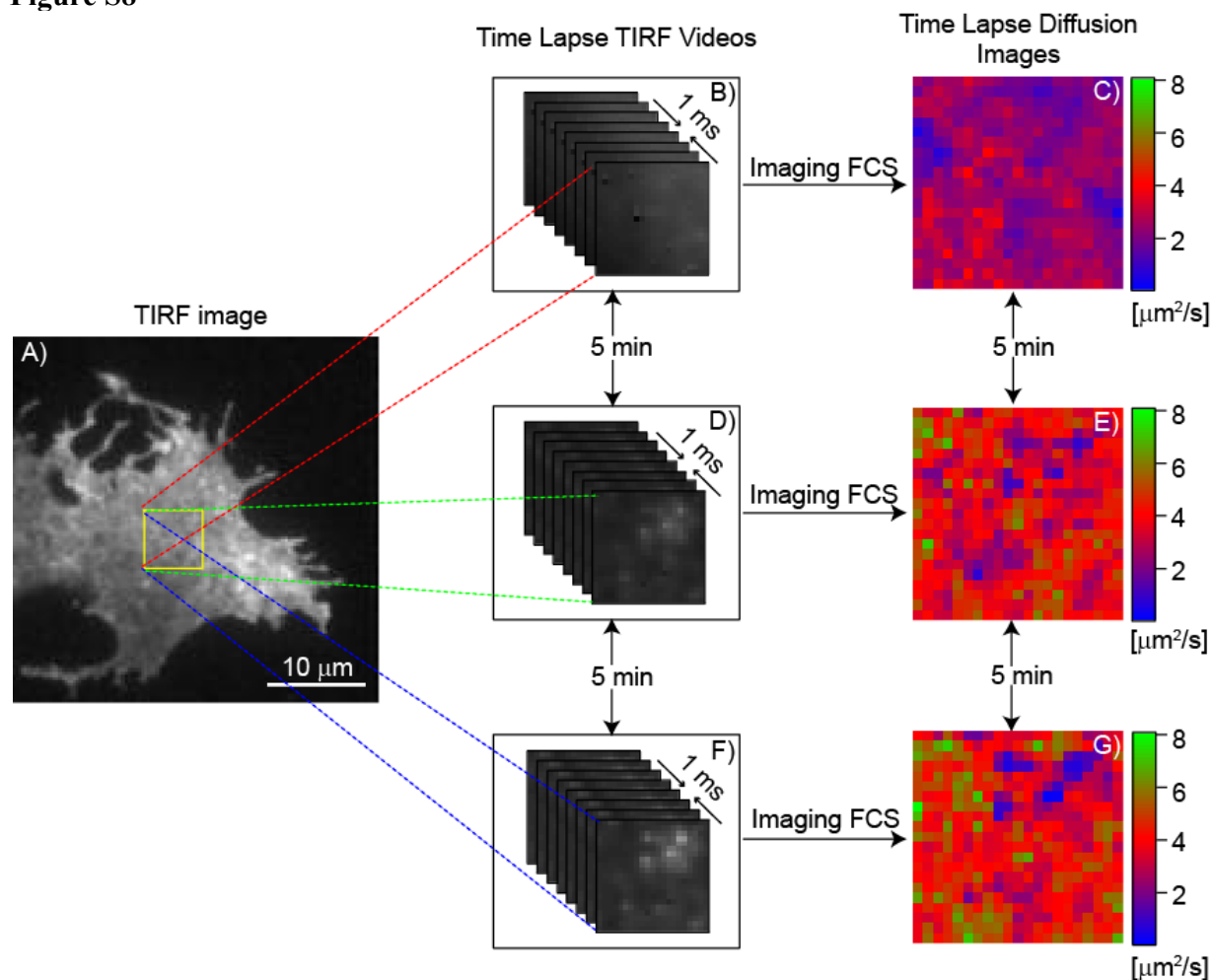
**Figure S6.** Interaction of 1  $\mu\text{M}$  unlabelled hIAPP with REV and RLV. (A) ACFs of the REV before (brown) and after addition of 1  $\mu\text{M}$  hIAPP. (B) ACFs of the RLV before (brown) and after addition of 1  $\mu\text{M}$  hIAPP. The diffusion time of both REV and RLV increase (ACFs widen) upon addition of 1  $\mu\text{M}$  hIAPP. However, one would expect the diffusion time to decrease for the REV sample if hIAPP would have formed pores (Fig. S5) while that of RLV would have remained constant. Thus we conclude that hIAPP does not form pores in the vesicles. Rather, the vesicles aggregated upon peptide addition.

Figure S7



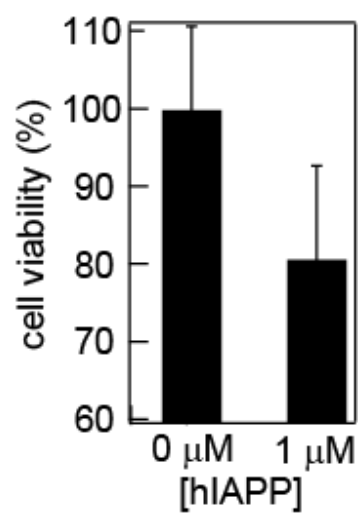
**Figure S7.** Disruption of REV by 40  $\mu$ M unlabelled hIAPP. (A) The top panel shows the change in diffusion time of rhodamine entrapping vesicles (REV) over time on addition of 40  $\mu$ M hIAPP. hIAPP remains as mostly aggregated at this concentration (as shown in Figure S1D). It shows that REVs first aggregate (green) and then rupture (red) as indicated by the release of the entrapped dyes. To corroborate the results obtained from FCS measurements, TEM micrographs are also shown: LUVs before (B) and after (C) addition of 40  $\mu$ M hIAPP. Image (C) also shows the fibrillar structure of hIAPP at this concentration.

Figure S8



**Figure S8.** Principle of time lapse diffusion imaging (FCS movie). (A) A region of interest (ROI) on the plasma membrane is first chosen (yellow box in figure A). (B) An image series (TIRF video) of 50,000 stacks is acquired with 1 ms time resolution from the selected ROI (the detailed description of data acquisition is provided in the 'ITIR-FCS data acquisition and data analysis' section of the supplementary information). (C) The autocorrelation functions (ACF) are calculated from the temporal intensity fluctuations of each pixel in the ROI followed by fitting with appropriate model. This provides diffusion coefficients at every pixel in the ROI and thereby a diffusion image is constructed. (D) and (F) The TIRF videos with identical acquisition conditions are taken in each 5 minutes. (E) and (G) The diffusion coefficient maps are obtained from the TIRF videos respectively. Overall, a series of diffusion coefficient images are obtained at each 5 minutes interval. This newly introduced diffusion image series is termed as 'FCS movie'.

**Figure S9**



**Figure S9.** MTT assay shows about 80% cell viability after 14 hr incubation with 1 μM hIAPP.

**Figure S10**

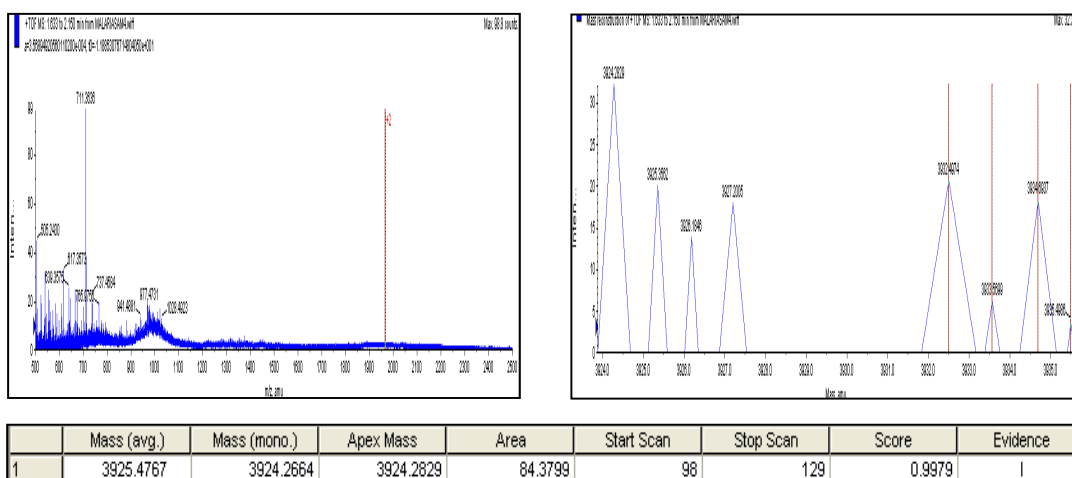


**Figure S10.** Electron Spray Ionization-Mass spectrometry in positive ion mode (ES<sup>+</sup>-MS) of purified hIAPP dissolved in Hexafluoro-2-propanol. Measurement was done on Applied Biosystems QSTAR (quadrupole time-of-flight mass spectrometer).

Expected Mol. wt. : 3903

Observed Mol. wt. : 3925 (Na<sup>+</sup>)

## Supporting information videos

**Video 1:** Time lapse TIRF image stack showing almost instantaneous formation of fluorescent structures on RhoPE labelled DOPC SLB upon addition of unlabelled hIAPP. The new structures emerge out from the SLB at 1.40 sec (frame = 14) (that marks the time where unlabeled hIAPP was added). The structures derive fluorescence from the fluorescently labelled (RhoPE) bilayer indicating that hIAPP extracts lipids from the membrane.

**Video 2:** TIRF videography showing Rho6G-hIAPP peptide over unlabelled DOPC SLB. The peptide appears to form a diffusing carpet-like structure over the membrane. Note that the peptide did carpet on the regions of membrane defect/collapse (dark region). The dark structures are not membrane domains since they are not completely circular and are too large in size to be obtained on a glass supported lipid bilayers. The diffusion coefficient of the carpet is much higher than the lipid diffusion inside the membrane (Fig. S2).

**Video 3:** This movie is created by merging diffusion maps generated by ITIR-FCS at different time intervals after treating DiI-C<sub>18</sub> stained cell membrane with 1  $\mu$ M unlabelled hIAPP. Brightly fluorescent structures are formed that exhibit regions of diffusion barriers. At shorter time points (0-20 minutes) the overall diffusion coefficient increases. At longer time points (> 20 minutes) the slow diffusion features start appearing (more pixels with slow diffusion coefficient). The spatially averaged (over all 441 pixels) diffusion coefficients at longer time points have large standard deviation (~95% at the last time point) since pixels with both slow and fast diffusion coefficients were averaged. This reveals the hIAPP-induced diffusion heterogeneity of the live cell membrane over long incubation time as also shown by FCS diffusion law analysis (Fig. 3D).

## Acknowledgement

Aseem Mishra acknowledges Wellcome Trust-DBT IA Early Career Fellowship. Aseem Mishra, Ashraf Ali and Virander Singh Chauhan thank ICGEB core grant. Nirmalya Bag thanks National University of Singapore Graduate Scholarship. Thorsten Wohland acknowledges the funding by the Ministry of Education Singapore (MOE2012-T2-1-101). The authors thank Darilyn Yap Hui Xin for providing culture of mammalian cells. Aseem Mishra thanks DIT, India for home built FCS (No. 12(4)/2007-PDD).